Supplementary Materials

Exploring Air stability of All-Inorganic Halide Perovskites in the presence of Photogenerated Electrons by DFT and AIMD studies

Ming-Quan Cai[†], Dhana Lakshmi Busipalli[†], Shi-Hong Xu, Santhanamoorthi Nachimuthu[*], and Jyh-Chiang Jiang*

Department of Chemical Engineering, National Taiwan University of Science and Technology, Taipei 106, Taiwan, R.O.C.

Corresponding authors:
santhanamoorthi@gmail.com (S.N)
jcjiang@mail.ntust.edu.tw (J.C.J)

Telephone: +886-2-27376653. Fax: +886-2-27376644

[†]These authors contributed equally to this work

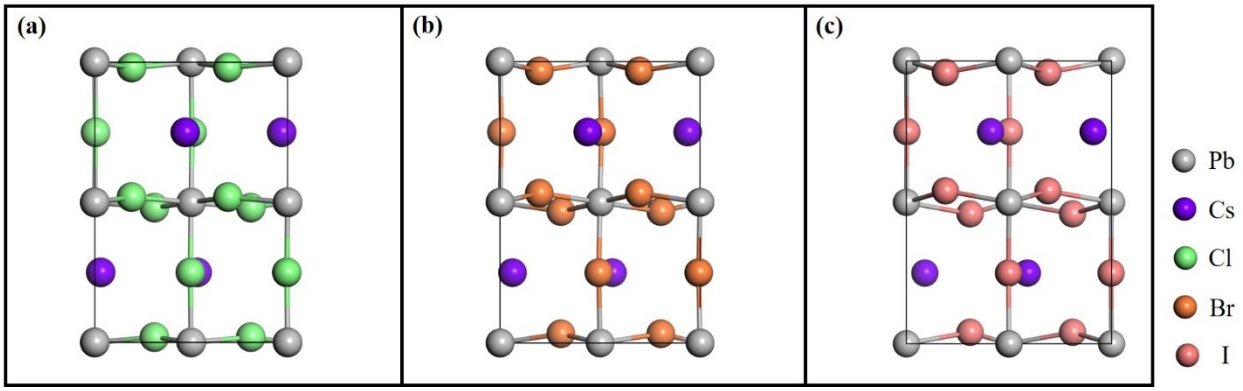

Figure 1S. Optimized bulk model of orthorhombic phase of (a) $CsPbCl_3$, (b) $CsPbBr_3$, and (c) $CsPbI_3$ perovskites

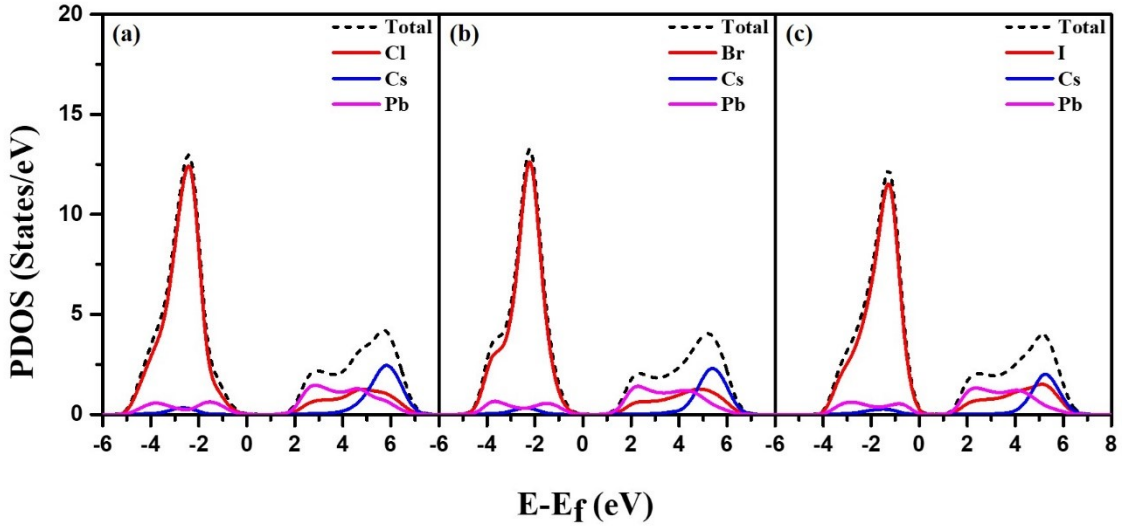

Figure 2S. Total and projected density of states of the bulk orthorhombic phase of (a) $CsPbCl_3$, (b) $CsPbBr_3$, and (c) $CsPbI_3$ perovskites.

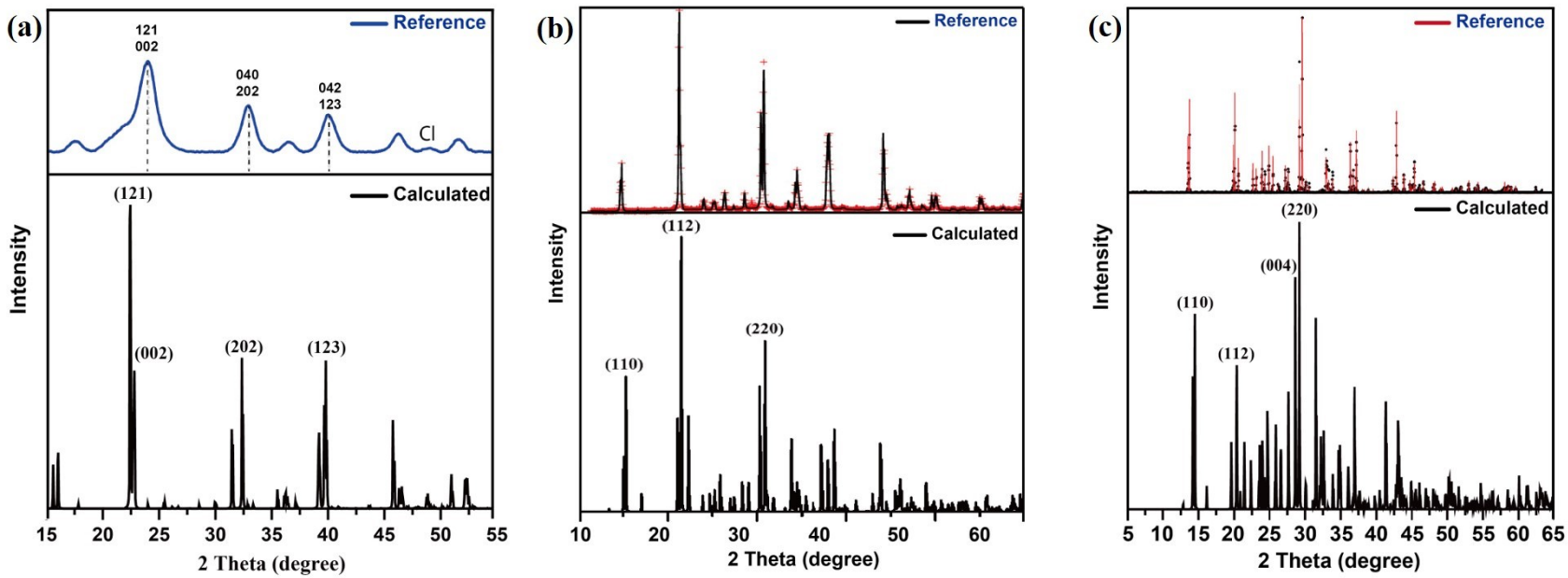

Figure 3S. Simulated XRD patterns of the bulk orthorhombic phase of (a) $CsPbCl_3$, (b) $CsPbBr_3$, and (c) $CsPbI_3$ perovskites along with their experimental data.

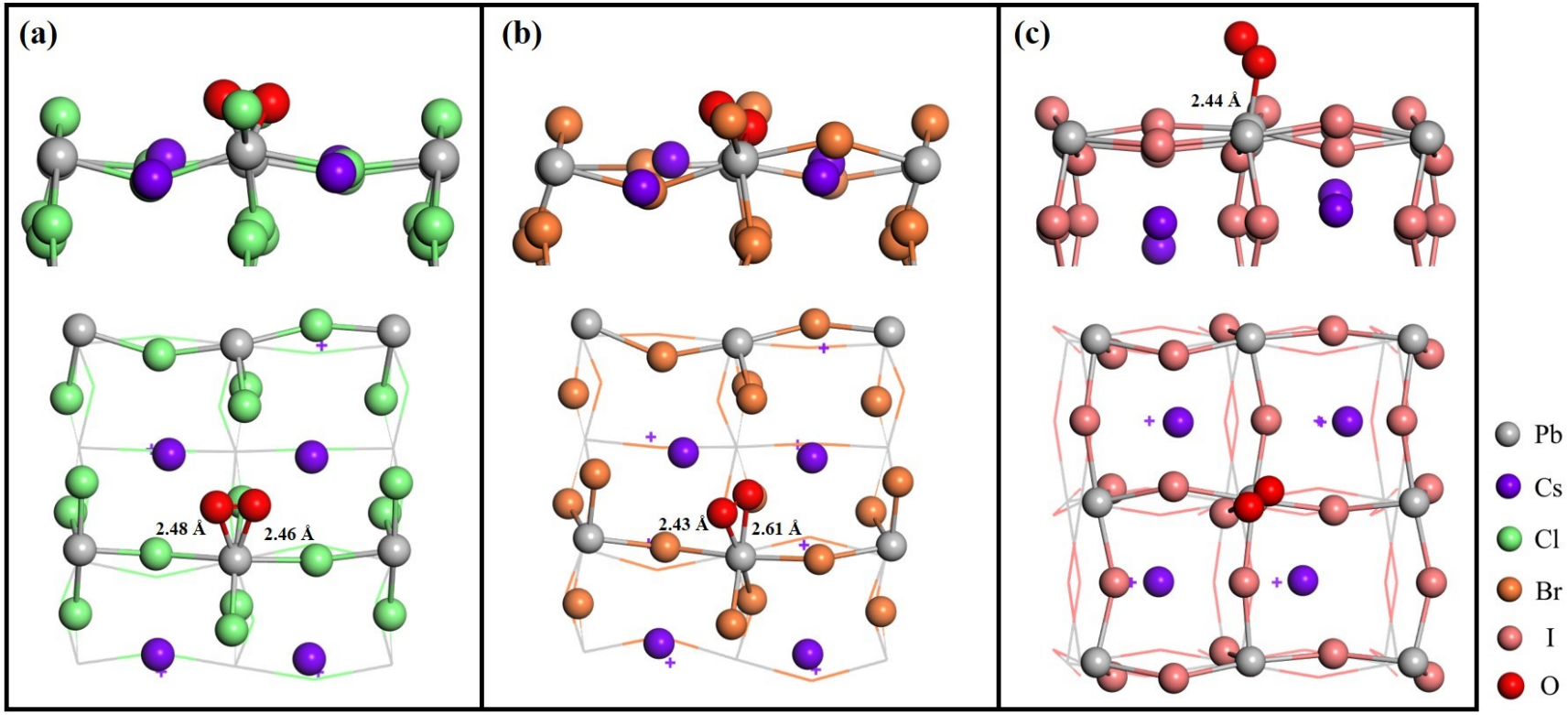

Figure 4S. Side and top views of optimized geometries of most stable adsorption configuration of O_2 on (a) $CsPbCl_3$ (121), (b) $CsPbBr_3$ (112), and $CsPbI_3$ (220) perovskite surfaces with the photogenerated $1e^-$.

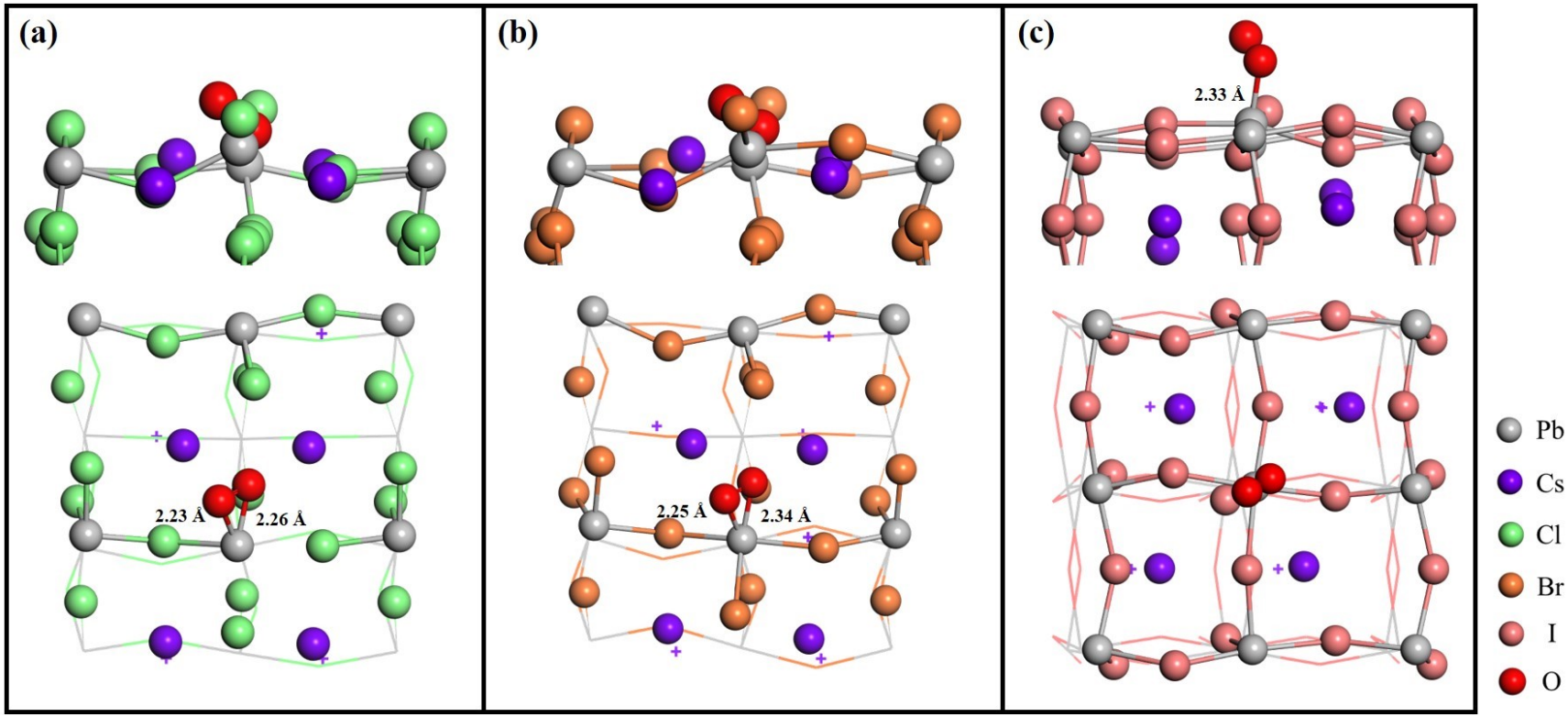

Figure 5S. Side and top views of optimized geometries of most stable adsorption configuration of O_2 on (a) $CsPbCl_3$ (121), (b) $CsPbBr_3$ (112), and $CsPbI_3$ (220) perovskite surfaces with the photogenerated $2e^-$.

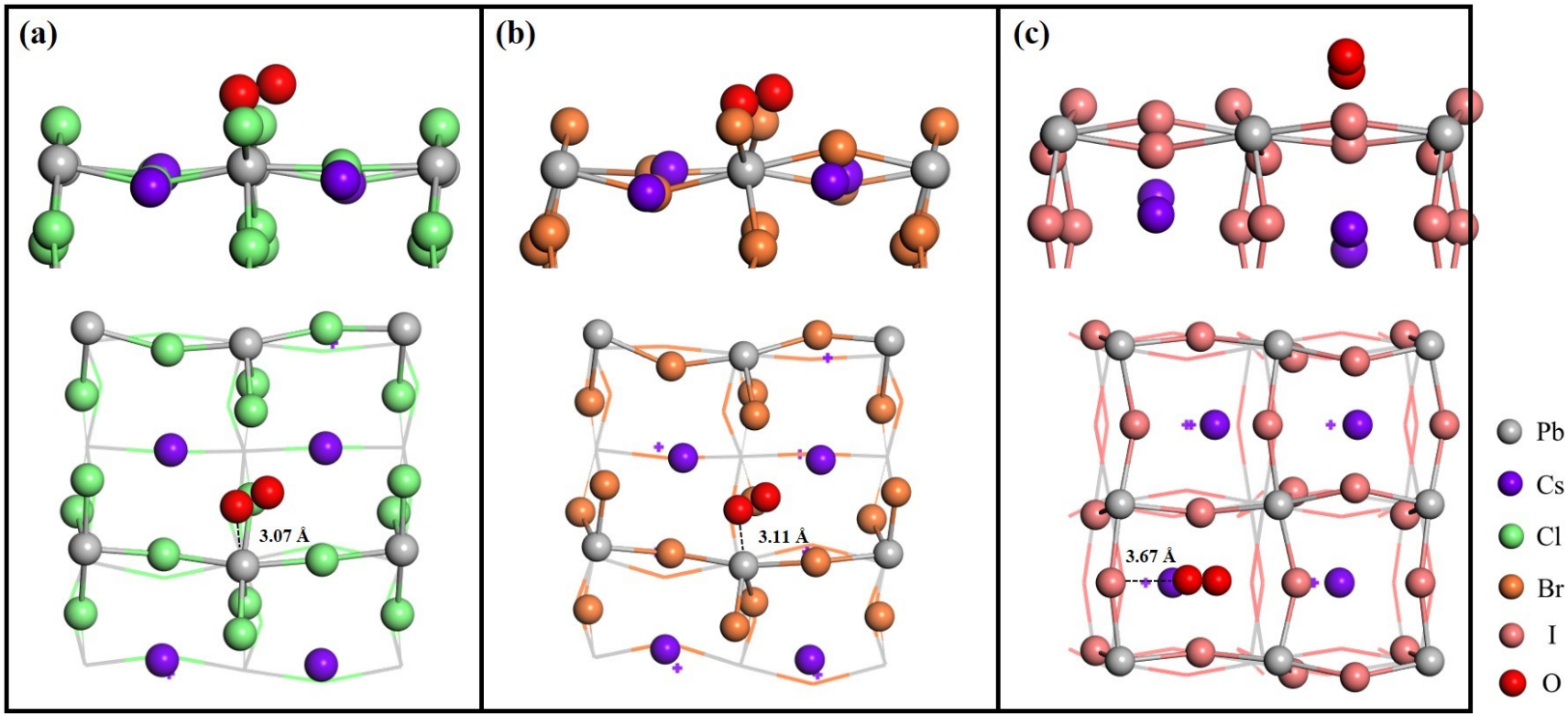

Figure 6S. Side and top views of optimized geometries of most stable adsorption configuration of O_2 on (a) $CsPbCl_3$ (121), (b) $CsPbBr_3$ (112), and $CsPbI_3$ (220) perovskite surfaces with the photogenerated $1h^+$.

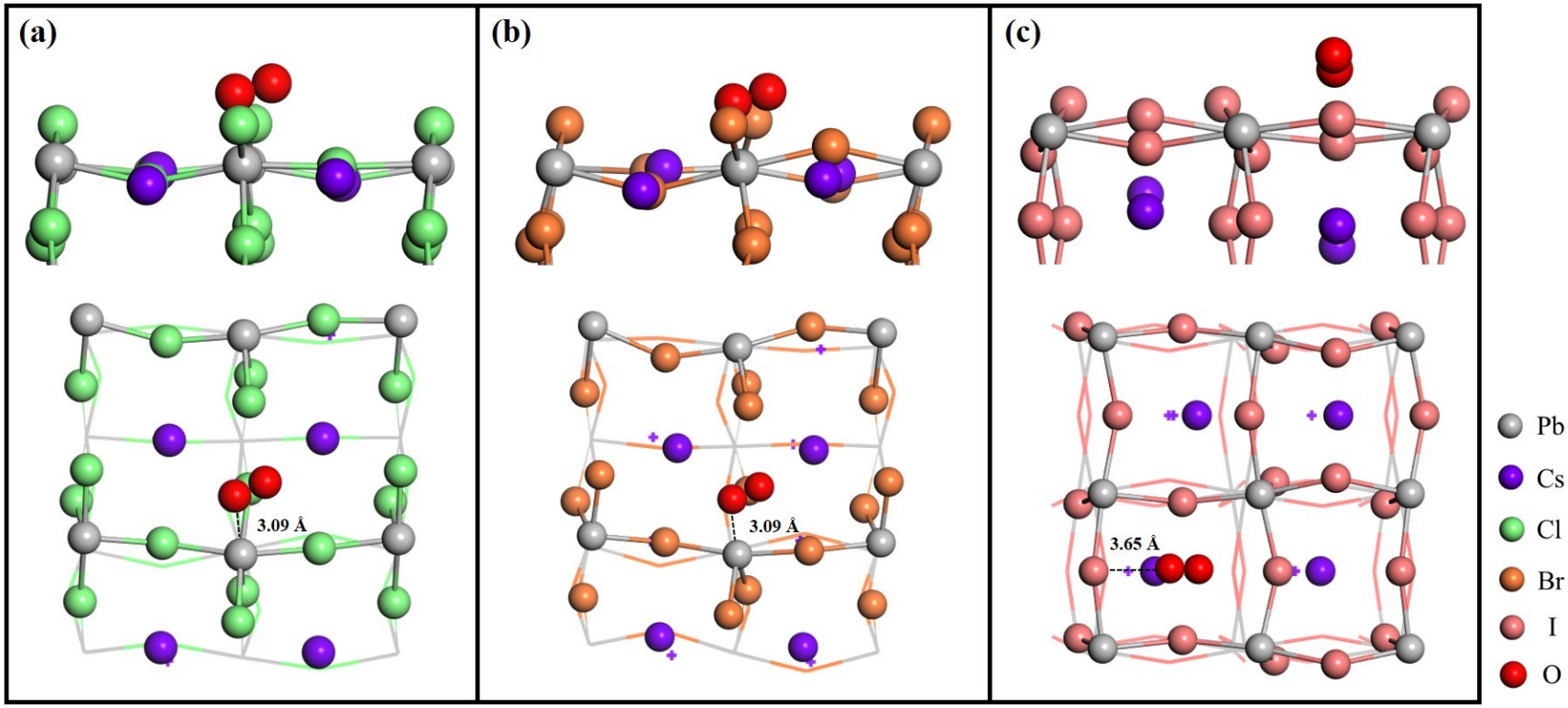

Figure 7S. Side and top views of optimized geometries of most stable adsorption configuration of O_2 on (a) $CsPbCl_3$ (121), (b) $CsPbBr_3$ (112), and $CsPbI_3$ (220) perovskite surfaces with the photogenerated $1h^+$.

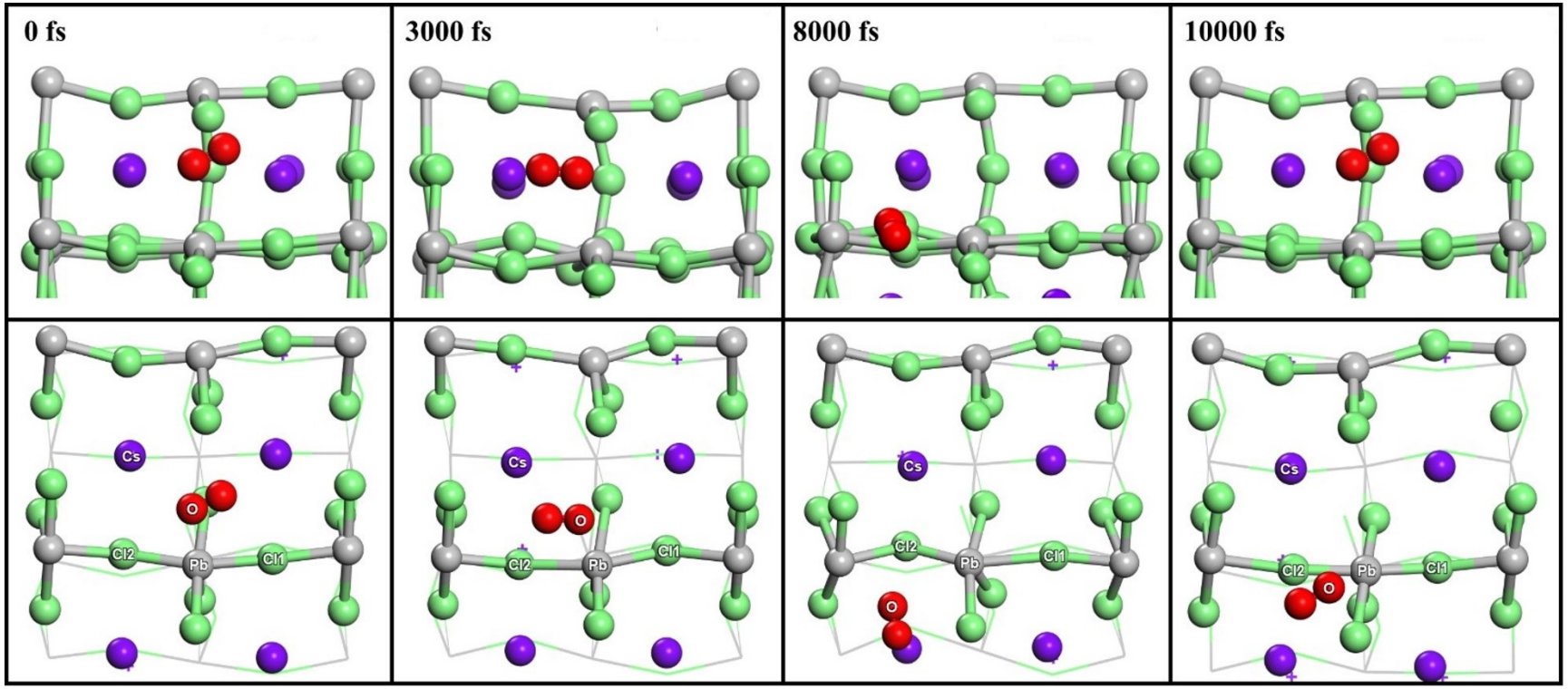

Figure 8S. Top and side views of selected snapshots of the AIMD trajectory at different simulation times for O_2 adsorbed on the $CsPbCl_3$ (121) perovskite surface in neutral.

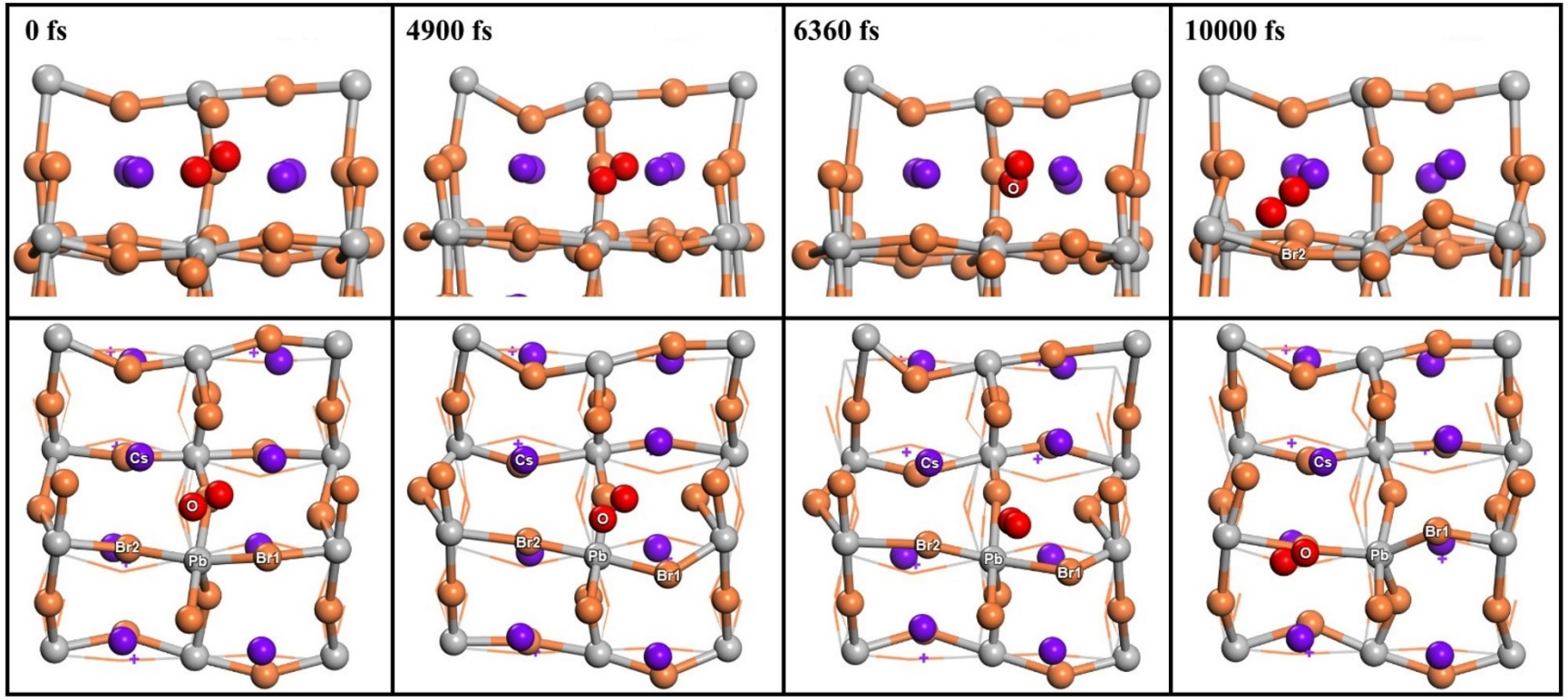

Figure 9S. Top and side views of selected snapshots of the AIMD trajectory at different simulation times for O_2 adsorbed on the $CsPbBr_3$ (112) perovskite surface in neutral.

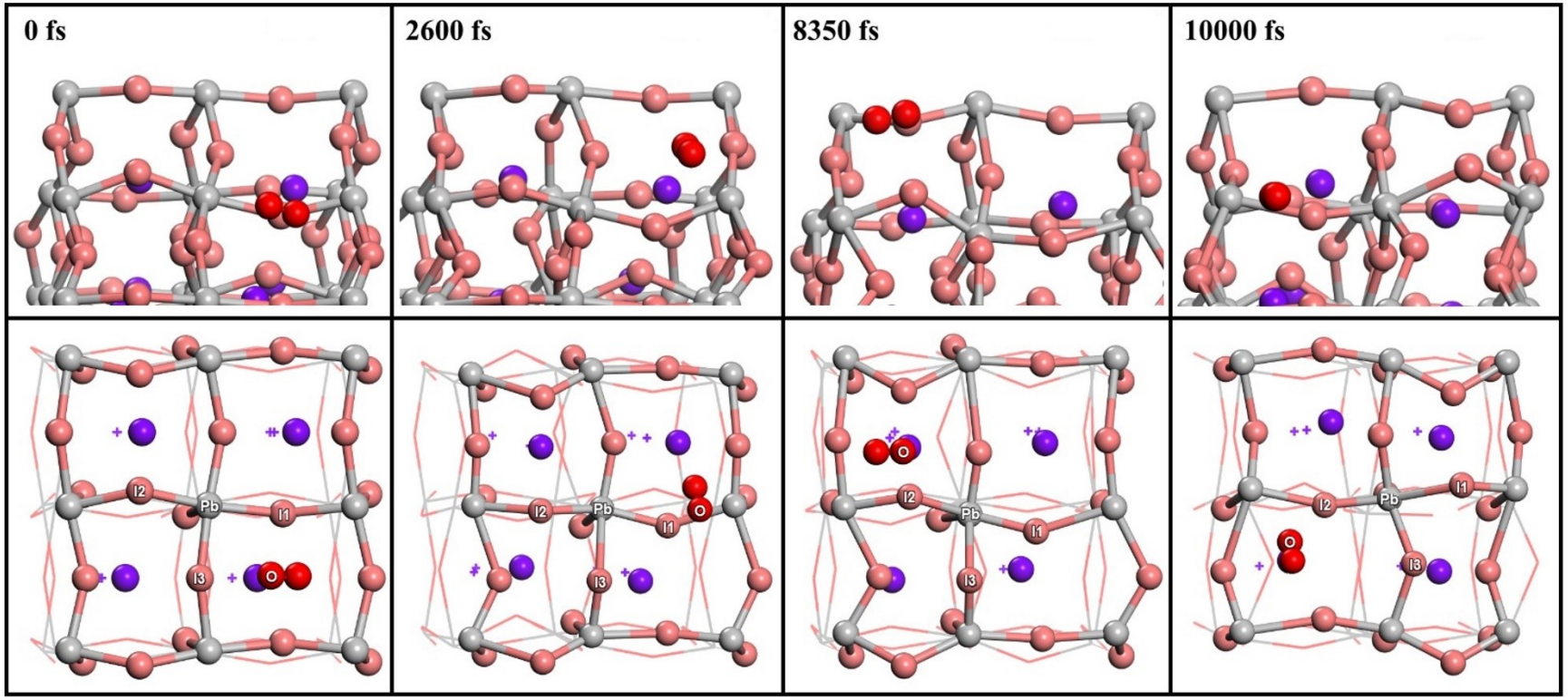

Figure 10S. Top and side views of selected snapshots of the AIMD trajectory at different simulation times for O_2 adsorbed on the $CsPbI_3$ (220) perovskite surface in neutral.

Table 1S. Calcualted O_2 adsorption energies (E_{ads} in eV) for the least stable configurations on the $CsPbX_3$ (X=Cl, Br, I) perovskite surfaces.

X	Site	E_{ads}
Cl	Top_Cs	-0.15
	Top_Cl	-0.07
	Hollow	-0.16
Br	Top_Cs	-0.13
	Top_Br	-0.04
	Hollow	-0.08
I	Top_Pb	-0.16
	Top_I	-0.14

Table 2S. Calculated O_2 adsorption energies (E_{ads} in eV) on the $CsPbX_3$ (X=Cl, Br, I) perovskite surfaces with four molecular layers, the shortest adsorption distance of O_2 to the surface (d_{O_2-S} in Å), and the O_2 interatomic distances (d_{O-O} in Å).

X	$\mathbf{E_{ads}}$	d_{O_2-S}	d_{O-O}
Cl	-0.20	3.04	1.237
Br	-0.22	3.05	1.240
I	-0.17	3.71	1.235